Laboratory PIV measurements of wave breaking on a beach

O. Kimmoun, H. Branger and B. Zucchini**
ESIM, Marseilles, France
*IRPHE, CNRS, Marseilles, France

ABSTRACT

Experiment were conducted in the ESIM wave tank in Marseilles in order to study the space/time evolution of the flow field under waves breaking on an 1/15 beach slope. Fluid particles velocities were measured at different depths, before, during and after the breaking event using the Particle Imaging Velocimetry (PIV) technique. The mean and fluctuant components of the flow were calculated.

KEY WORDS: wave; wave breaking; PIV; measurements; wave tank; experiment; shoaling; reverse flow.

INTRODUCTION

Understanding the kinematics and dynamics of the flow in the surf zone is a major area of the hydrodynamics research which concerns coastal engineers, marine development and transport of marine sediment. Open field measurement of instantaneous flow velocity under breaking waves are very difficult to investigate. It is not easy to install an experimental set up on a beach where large waves are breaking. Experiments in a wave tank are a more easy way to investigate physical processes during wave breaking due to shoaling. A central problem in the modeling of waves in the surf zone is the proper quantification of the mass flux inherent in a breaking wave. The magnitude and the fluctuations of the reverse flow located near the bottom and directed off-shore are yet not well known. In an other extent, space/time flow measurements in well-controlled wave-tank environment are required to tune numerical models.
Peregrine (1983) and Battjes (1988) made a complete review of the surf-zone dynamics and the related physical mechanisms during wave breaking on beatches. Jansen (1986) has employed photographic flow visualization techniques to describe the flow structure evolution in the breaking process. Nadakoa et al. (1989) used a 2D optic fibre to make Laser Doppler Velocimetry (LDV) measurements in a tank under spilling breakers. They found obliquely descending eddies that play a significant role in momentum transport. Ting and Kirby (1994, 1995, 1996) carried out a series of experiments with LDV on turbulent transport due to wave breaking on 1/35 slope beaches. They found the turbulent kinetic energy transport to be landward under spilling breakers, and seaward under plunging breakers. They also found that the turbulent transport scale is dominated by the large scales. Petti and Longo (2001) made turbulence laboratory experiments in the swash zone on a 1/10 concrete beach. With LDV equipment, they described the wave front dynamics and the turbulence micro and macro scales more precisely during the run-up phase following the breaking event. LDV and hot film measurements are "point after point" measuring techniques and they do not allowed to determine the spatial velocity field. The Particle imaging velocimetry technique (PIV) is much more efficient in order to better understand the evolution of wave breaking on a beach. The PIV technique was employed by several authors for deep water breakers (Skyner (1996), Perlin et al 1996, Lin and Rockwell 1995). They found that breaking led to regions of concentrated vorticity. But breaking of waves in infinite depth differs qualitatively from breaking running on beatches since the region directly mixed down by the breaking is of finite extent. Chang and Liu (1998) measured fluid particles velocities in the overturning jet of a breaker in a shallow water. They found that the velocity at the tip of the jet reached 1.7 times the phase velocity of the wave. Recently, Govender et al (2002), presented roller geometries and phase ensemble averaged velocity fields under spilling and plunging waves breaking in a laboratory surf zone with a slope of 1/20. They made use of the bubble structures in the application of digital correlation image velocimetry procedure (PCIV), which is slightly different from PIV measurements. For wave breaking on slope beach, we do not know yet if the vertical mixing and evolution of turbulence is inhibited by the presence of the bottom of the channel.
This paper presents experimental results of periodic breaking waves in in the ESIM wave tank in Marseilles using a Particle Image Velocimetry system. We present the experimental arrangement and the results. The magnitude of the mean return flow, as function of the depth and distance from the beach is measured.

EXPERIMENTAL ARRANGEMENT

Experiment were conducted in the ESIM glass-walled wave tank in Marseille. A schematic of the experimental set up is shown on figure 1. The tank is 16.8 m long, 0.65 m width and the water depth was 0.80 m

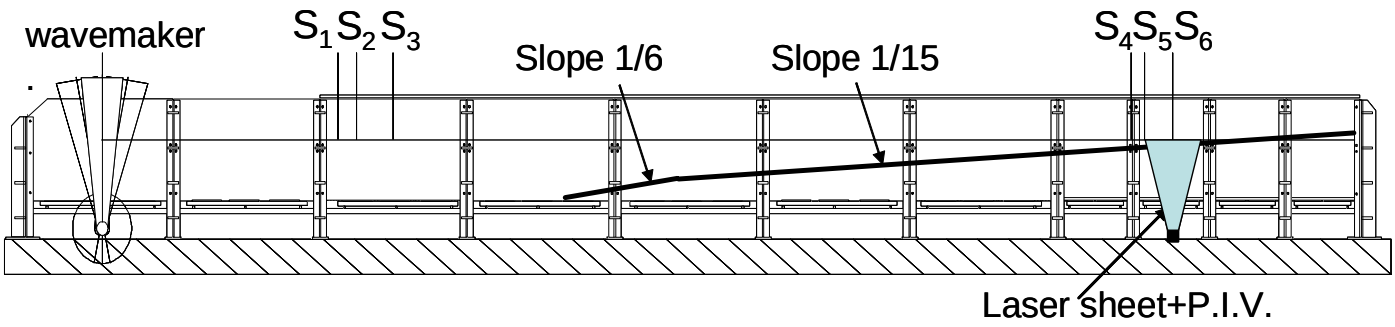

Figure 1 : Experimental set-up.

near the computer controlled flap type wavemaker. Wave shoaling and breaking then occurred over a 1/15 polyvinyl plastic slope beach. Water elevation was measured with 6 resistance wire wave gauges located at different locations near the wave maker and in the breaking region. The sampling frequency was 100 Hz for each channel. Different regular monochromatic wave conditions were performed, with wave period ranging from 0.6 s to 2.0 s, and amplitude ranging from 3.0 cm to 5.0 cm. For each series, we waited 50 wave-period before starting data acquisition, thus avoiding transitional start-up and non-homogenous conditions.

The velocity field in the breaking region was measured using PIV technique. PIV is perhaps the most versatile measurement technique currently available for measuring instantaneous flow fields (Adrian 1991 for a review). The PIV procedure consists in seeding, illuminating, taking camera pictures and processing images. The water in the channel was seeded with 8 μm neutrally buoyant silver coated hollow glass sphere. A stroboscopic light sheet was generated by a twin Nd-YAG 300 mJ laser system. Pairs of digital images (1018x1008 pixels2, 256-level grey scale) were recorded using a double frame digital Kodak Megaplus ES1.0 camera . The time between two pair of images was set to 10 ms. The delay between the two images inside the pair was 100 ms. The actual field of view was about 37x37 cm, which corresponds to a scale of 0.036 cm/pixel.

We used the PIV image processing software developed at IRPHE (Meunier and Leweke, 2003). It is based upon a recursive multi-pass cross-correlation technique in the spectral domain, with window shifting and deformation, taking into account the velocity gradient. The interrogation window was 64x64. pixels. We used a 50% window overlap. A local median filter technique was applied to the computed velocity. This procedure, associated with a Gaussian filtering, allows the correlation peaks to be as narrow as possible. We developed also an automatic wave profile detection procedure, in order to invalidate all the velocity vectors located above the water.

It was not possible to move the PIV illumination and camera system all along the tank. In order to acquire PIV pictures at different locations (i.e. at different stages of wave breaking : before, during and after the breaking process), we modified the depth water in the tank without moving the camera: a decrease of 1cm in water depth is equivalent to a shift of 15 cm of the camera and illumination system towards the shoreline.

RESULTS

Before breaking : comparison with analytical Fenton formulation.

In order to validate our experimental wave generation, measurement and data processing procedure, we measured the velocity field under regular waves before they reach the beginning of the slope bottom. Figure 2 presents an example of both theoretical and measured velocity field under an incident wave of 0.62 s period and 3.8 cm amplitude. The bottom is flat and the depth is 80 cm. The theoretical model is the Fenton analytical development up to the fifth order, which is a good approximate solution of the full Euler equation of traveling waves (Fenton 1990). In figure 2, the two velocity fields appear to be close to each other. In this example, the largest difference in modulus is located on the top left of the figure, and the largest error in flow direction is located on the middle right of the figure. Comparisons were made at different phases of wave propagation. We compared the velocity field over several wave periods and wavelengths: the RMS relative error on the velocity modulus is equal to 17 %, and the RMS absolute error in velocity direction is 7 degrees. The overall agreement between model and experiment is rather good.

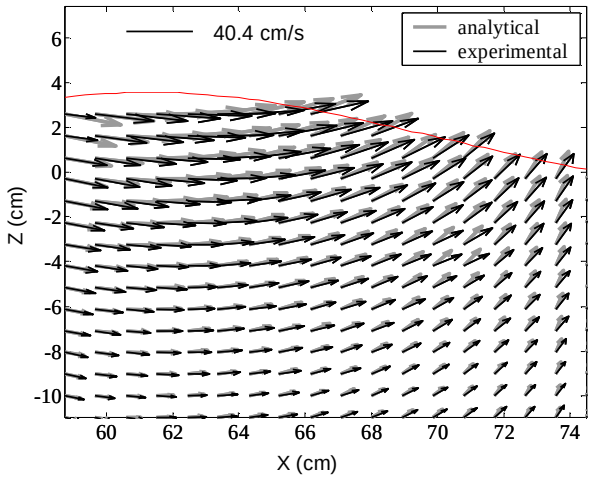

Figure 2 : Comparison between experimental results and analytical formulation (Fenton 1990) for regular waves over flat bottom. Z=0 cm is the water level at rest, and X=0 cm is the location of the previous wave crest.

Instantaneous Velocity fields for breaking waves

Figure 3 shows examples of instantaneous PIV velocity fields under 1.6 s incident waves breaking on the beach. The altitude Z=0 is the

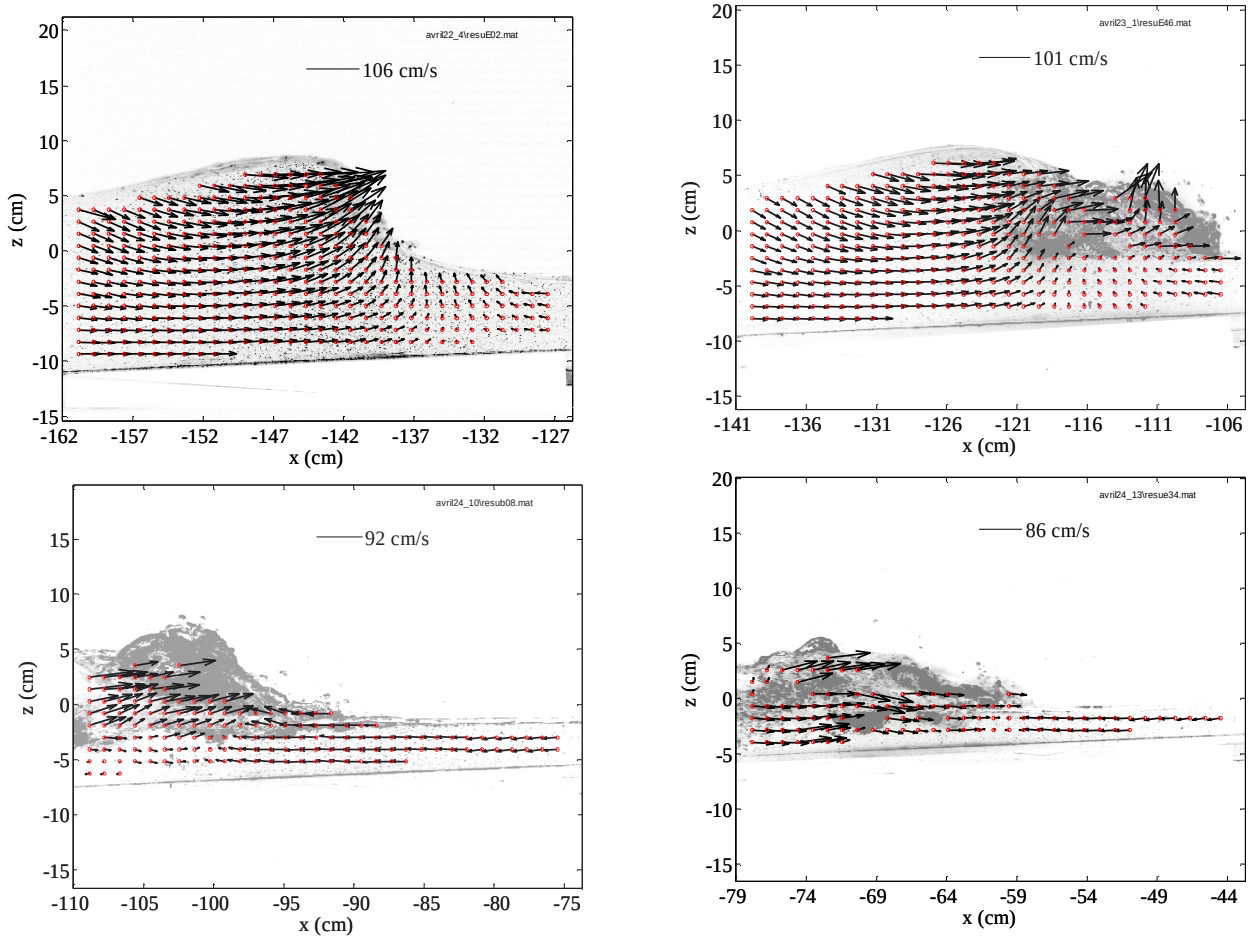

Figure 3 : Instantaneous PIV velocity field under an incident 1.6 s wave. Z=0 cm is the water level at rest. X=0 cm is the location of the shore line for water level at rest, i.e. without wave. A reference velocity scale is indicated for each sub-image.

water level at rest. The X-axis is the distance from the shoreline. For clarity, only 1/4 of the computed vectors are shown. The wave begins to break with a vertical front slope which is transformed into a curtly plunging breaker with a curved jet on the top of the crest and high velocities on the front. The lip of the wave hits the water and generates a splash-up. The breaker is then transformed into a spilling breaker, which propagates to the right. The wave runs up to the beach, then the flow turns back in the offshore direction. All the flow moves seaward until the next breaker comes. This return flow has probably an influence on the breaking of the next wave.

Mean Velocity fields

For each run we waited fifty wave periods before taking PIV pictures. Then we took hundreds of pictures. Data were acquired by series of two wave periods, and more than 12 series were acquired without stopping the wave-maker. Mean and fluctuant velocities were then computed. The phase φ of the waves was computed by means of Fourier transforms. In order to be sure that a quasi-equilibrium state was obtained, we put on the same graph, in figure 4, phase-locked time series of vertically averaged horizontal velocity, $\langle U(x,t)\rangle_Z$, for 12 successive couples of waves (each couple has a specific marker type).

$\langle U(x,t)\rangle_Z$ is defined by:

$$\langle U(x_o,t)\rangle_Z = \frac{1}{d+\eta}\int_{-d}^{\eta} u(x_o,z,t)dz$$

where d is the local depth, η the free surface and t is the time. In this figure, the wave period is 1.6 s and x_o is equal to -121 cm, i.e. at the location where the waves break. The plots in figure 4 are phase-locked: they all start at phase $\varphi = 0$, the location of the wave trough. The dark line is a spline interpolation of all the data. This figure shows that the wave field is somehow periodic with a quasi-equilibrium state without significant transient low frequency effect. It means that fifty wave periods were enough to wait before acquiring PIV data.

An example of time-average flow velocity, $\langle U(x,z)\rangle_T$, for 1.6s period waves, is presented on figure 5. $\langle U(x,z)\rangle_T$ is defined by :

$$\langle U(x,z)\rangle_T = \frac{1}{NT}\int_0^{NT} u(x,z,t)dt$$

where T is the wave period, and N the number of waves.

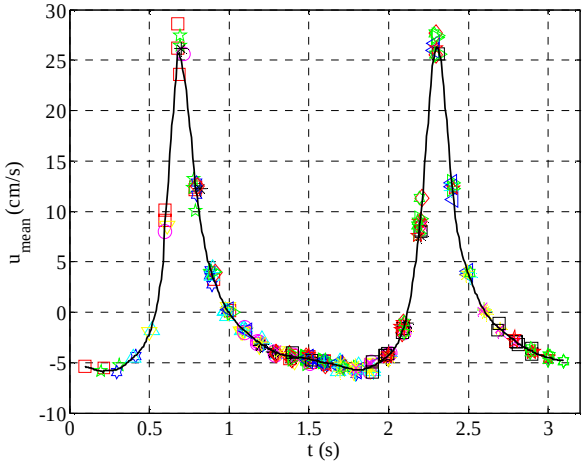

Figure 4 : phase-locked time series of the vertically averaged horizontal velocity, $\langle U(x,t)\rangle_Z$, at location xo=-121 cm. The wave period is 1.6 s. Markers represent data from twelve successive pair of waves, starting from phase $\varphi = 0$ (trough). The dark line is a spline interpolation.

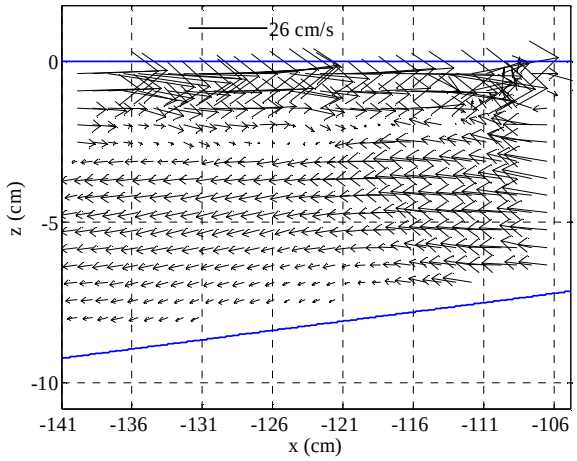

Figure 5 : Example of time average flow field $\langle U(x,z)\rangle_T$ for wave period 1.6 s. Z=0 is the water level at rest. X=0 is the location of the shore line (where d=0).

Only velocity vectors located under the water level at rest are presented. Above the altitude z=0, there is no water when the trough of the wave is propagating, so it is unrealistic to compute a time average velocity in a location where half of the time there is no water. The mean flow near the water level at rest is characterized by a strong current at the surface directed shoreward, and just under it by a mean reverse current direct seaward. This reverse flow appears also to be slightly downward, parallel to the bottom line. The zero-mean flow is approximately located at z=-d/3. In this figure, the mean reverse flow appears to be stronger on the right size, i.e. near x= -110 cm. On a real sand beach, sand particles, if any, will propagate from the shore line to deep ocean.

In order to quantify the magnitude of the reverse flow all along the bottom line, we present in figure 6 the magnitude of the mean flow at different iso-distance from the bottom. For example, the upper curve of

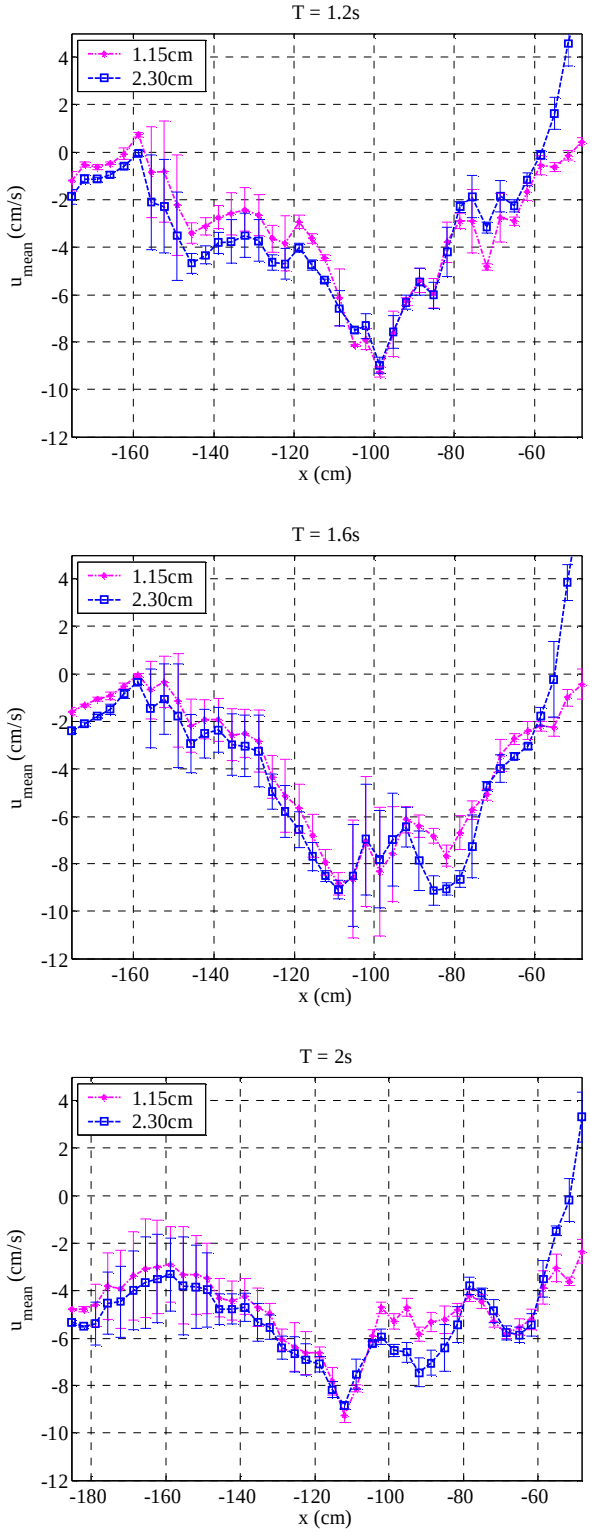

Figure 6 : Magnitude of the reverse flow at iso-distance from the bottom line (respectively 1.15 cm and 2.30 cm from bottom.). Incident wave with period 1.2s (top figure) 1.6 s (middle) and 2.0 s (bottom.). The x-axis is the distance from the shore. Curves represent the temporal mean velocity. Error bar is two standart deviations.

figure 6 is the temporal mean intensity of the flow, at an 1.15 cm iso-distance from the bottom line, for incident waves with a 1.2 s period. The x-axis is the distance from the shore. Each value was computed for numerous waves. The error bars are two standart deviations. Far from the shore the mean flow is negative, i.e. seaward, and weak. The mean flow is around 0 cm/s near x=-160 cm, i.e. before wave breaking. Then the absolute magnitude of the velocity increases up to approximately |-9| cm/s. The maximum of intensity is reached near x=-100 cm for 1.2 s wave and near x=-113 cm for 2 s wave, which is the location of the splash-up breakdown after the overturning wave breaking. Closer to the shore, the velocity magnitude decreases rapidly towards zero, then it turns to be positive, i.e. onshore. At that location, close to the mean water level, the velocity increases rapidly as the depth decreases, because the rolling breaking-wave, which is located more near the surface, moves towards the shore (see figure 3 for low depth).

Turbulent part

A Reynolds type decomposition is adopted to decompose the instantaneous velocity vectors into a mean time averaged part along with the turbulent fluctuations $\vec{U}(x,z,t) = <\vec{U}(x,z)>_T + \vec{U}'(x,z,t)$. The turbulent kinetic energy is the mean square of the velocity fluctuations. Since the PIV measurements provides only two components of the flow: $\vec{U} = (u,w)$, the mean turbulent kinetic energy, $<q'^2(x,z)>_T$ is estimated using the standard approximation for the surf zone flow (Svendsen 1987, Govender et al 2002) :

$$<q'^2(x,z)>_T = \frac{4}{3}\frac{(<u'^2(x,z)>_T + <w'^2(x,z)>_T)}{2}$$

u' and w' being the horizontal and vertical fluctuation components of the flow field. Figure 7 presents a map of the mean turbulent kinetic energy in the location where the mean reverse flow is maximum. High values of turbulent kinetic energy are found near the bottom. This could have some implications in sediment transport, because the probability of sediment movement is related not only with the intensity of the mean flow but also with the kinetic turbulent intensity near the bottom boundary layer (Dancey and Diplas 2003).

CONCLUSIONS

Experiments were conducted in a glass wave-tank in order to measure instantaneous and mean flow field and fluctuations for regular incident waves shoaling on a 1/15 rigid slope beach. Water elevation was measured with several wave gauges, and a PIV system was set up to evaluate space/time evolution of velocity field. The main difficulties were to automatically detect the free surface during wave breaking, and to avoid laser light reflexion by the air bubbles toward the camera. The PIV system is quite suitable for investigations of various unresolved aspects of wave breaking in shallow water regions. We obtained velocity vectors even in the spash-up region, and in the rollering part of the breaking near the shore. The mean flow is sea-ward near the bottom, and shore-ward near the surface. There is a maximum value of the return flow which seems to be located near the splash-up breakdown, downstream the first breaking, with high level of turbulent intensity. We are now investigating turbulence energy budgets.

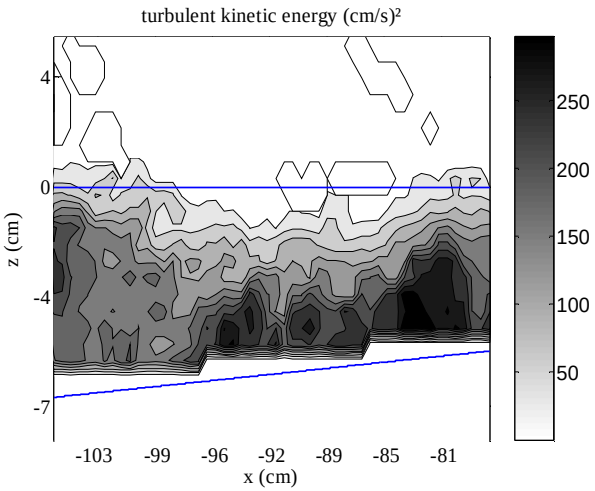

Figure 7 : Mean turbulent kinetic energy $<q'^2(x,z)>_T$ for wave period 1.6 s near the location where the mean reverse flow is maximum.

ACKNOWLEDGEMENTS

This work was supported by French CNRS PATOM Program.

REFERENCES

- Adrian R J, (1991), "Particle-imaging techniques for experimental fluid mechanics", *Ann. Rev. Fluid Mech.,* vol 23, 261-304.
- Battjes A, (1988), "Surf-zone dynamics", *Ann. Rev. Fluid Mech.,* vol 20, 257-293.
- Chang K A and Liu P L, (1998), "Velocity, acceleration and vertical vortex under a breaking wave", *Phys Fluids,* vol 10, 1, 327-329.
- Dancey C L and Diplas P, (2003), "The probability of sediment movement at the threshold of motion and time dependent fluid processes", in *"Sedimentation and Sediment Transport", Proceedings of the Symposium*, Monte Verita, Switzerland, San Diego Tech. Book, Inc., Albert Gyr Edt, 57-61.
- Fenton J D, (1990), " Non linear wave theories", in *The sea : Ocean Engineering Sciences*, vol 9, part A, Eds Le méhauté, 3-25.
- Govender K, Mocke G and Alport M, (2002), "Video-imaged surf zone wave and roller structures and flow fields", *Journ of Geophys. Research*, vol 107, 1029, 1-21.
- Jansen P C, (1986), "Laboratory observation of the kinematics in the aerated region of breaking waves, *Coastal Eng.,* vol 9, 453-477.
- Lin J C and Rockwell D, (1995), "Evolution of a Quasi-Steady Breaking Wave", *J. Fluid Mech.*, vol 302 , 29–43.
- Meunier P and Leweke T, (2003), "Analysis and treatment of errors due to high velocity gradients in particle image velocimetry, *Exp. In Fluids,* vol 35, In Press.
- Nadakoa K, Hino M, and Koyano Y, (1989), "Structure of turbulent flow field under breaking waves in the surf zone", *J. Fluid Mech.*, vol 204 , 359–387.
- Perlin, M, Bernal L, and He J, (1996), "An Experimental Study of Deep Water Plunging Breakers", *Physics of Fluids*, 8(9), 2365-2374.
- Perregrine D H, "Breaking waves on beatches", *Ann. Rev. Fluid Mech.,* vol 15, 149-178.
- Petti M and Longo S, (2001), "Turbulence experiments in the swash zone", *Coastal Eng.*, vol 43 , 1–24.

- Skyner D, (1996), "A comparison of numerical predictions and experimental measurements of the internal kinematics of a deep-water plunging wave", *J. Fluid Mech*, 315, pp 51-64
- Svendsen I A, (1987), "Analysis of surf-zone turbulence", *J. Geophys. Res.*, 92, 5115-5124.
- Ting C and Kirby J, (1995), "Dynamics of surf-zone turbulence in a strong plunging breaker", *Coastal Eng.*, vol 24 , 177–204.
- Ting C and Kirby J, (1996), "Dynamics of surf-zone turbulence in a spilling breaker", *Coastal Eng.*, vol 27 , 131–160.
- Ting C and Kirby J, (1994), "Observation of undertow and turbulence in a laboratory surf zone", *Coastal Eng.*, vol 24 , 51–80.